

# Computer-based design optimization of post-tensioned anchor for single-strand

Ah Sir Cho<sup>1a</sup> and Thomas H.-K. Kang<sup>\*2</sup>

<sup>1</sup>Department of Architecture, Dongyang Mirae University, 445 Gyoungin-ro, Guro-gu, Seoul, Republic of Korea

<sup>2</sup>Department of Architecture & Architectural Engineering and Engineering Research Institute, Seoul National University, 1 Gwanak-ro, Gwanak-gu, Seoul, Republic of Korea

(Received September 17, 2021, Revised October 19, 2021, Accepted October 20, 2021)

**Abstract.** In Korea, a 15.2-mm diameter strand is preferred for a post-tensioning (PT) method to reduce the total tendon and anchor number. However, the anchor for the Ø15.2-mm strand is large and sometimes inefficient while the anchor using the Ø12.7 mm single-strand is common in the United States. This study developed a post-tensioned anchor for Ø15.2-mm unbonded single-strand tendons to address the existing trend in domestic PT construction. The shape of the anchor is optimized to minimize the von Mises stress through a finite element analysis by varying the shape of the tubular body, bearing plate, and gussets. In addition, the design is also determined in consideration of a jacking device, accessories, and workability. ACI 423.7-14, on the other hand, requires the use of an encapsulation system, which is highly resistant to corrosion, for elevated floors. Therefore, the encapsulated anchor was also developed to enhance the durability of PT tendons and buildings.

**Keywords:** anchor; design optimization; encapsulation; finite element analysis; post-tensioning

## 1. Introduction

Structural concrete may be classified into reinforced concrete with passive steel reinforcement acting after substantial member deformation and prestressed concrete with active prestressing steel reinforcement (Kang and Wallace 2008, Ibrahim Ary and Kang 2012, Zhang *et al.* 2018, Choi *et al.* 2021). Prestressed concrete may be further classified into pre-tensioned concrete and post-tensioned concrete (Han *et al.* 2006, Kang and Ibrahim Ary 2012, Twigden and Henry 2019). A post-tensioning (PT) system applies compressive force to a concrete member by tensioning the prestressing steel in a duct or sheath previously buried in the concrete after it is hardened (Kim *et al.* 2018, Yim *et al.* 2018). Anchorages fix both ends of the tension element and convert the prestressing force into compressive force in the concrete member. The anchorage consists of an anchor and accessories such as pocket former, sleeve, and endcap.

In Korea, all PT anchorages used to import overseas which had hindered the PT market from

---

\*Corresponding author, Professor, E-mail: tkang@snu.ac.kr

<sup>a</sup>Assistant Professor, E-mail: ahsircho@dongyang.ac.kr

growing due to the high costs. Moreover, using  $\text{Ø}15.2$  mm stands is preferred to reduce the number of tendons. However, the size and dimension of the imported anchor for the  $\text{Ø}15.2$  mm strand are often too large and inefficient while the anchor for the  $\text{Ø}12.7$  mm strand, frequently used overseas, has a well-optimized size.

The authors developed a Korean domestic post-tensioned (PT) anchor for a  $\text{Ø}15.2$  mm unbonded single-strand for the first time (Cho *et al.* 2015). The design of the bare anchor, which is a single casting, was optimized through a finite element analysis. Furthermore, Cho and Kang (2018) improved the developed bare-type anchorage into an encapsulated anchorage for better long-term durability. Both bare and encapsulated anchors satisfied all kinds of domestic performance tests and have been applied in several buildings.

This study introduces the design process of developing from a bare PT anchor to an encapsulated PT anchor. Cho *et al.* (2015) and Cho (2021) introduced and summarized the process. However, this paper fully describes the whole development procedure using a finite element analysis that considers construction feasibility and economic efficiency.

## 2. Modeling criteria

A finite elemental analysis is suitable for the design of the bare anchor with a single material. The volume of the product is directly related to its price. To be competitive in the domestic market, it focused on minimizing the size as long as its performance was satisfactory. Its structural shape and strength were considered simultaneously by addressing the product fabrication and construction process at the same time. For the analysis, ABAQUS 6.10 was used.

For detailed design optimization, it is necessary to set up a few things that do not change; the shape of the wedge-contact surface, material properties, load, and boundary condition. In addition, the initial shapes and sizes of a tubular body and a bearing plate must be set to start analysis; even they can be altered in the subsequent process.

### 2.1 Wedge

Wedges are an essential component responsible for the primary stage of transmitting prestressing force to the anchor. Various high-level technologies, such as material, slope, length, depth and the number of treads, and heat treatment are required. Since developing the wedge itself is not the purpose of this study, the off-the-shelf products and the domestic wedges for the  $\text{Ø}15.2$



Fig. 1 Initial model of the tubular body (unit: mm)

Surface traction: 90 MPa

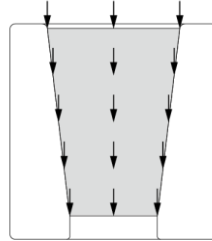


Fig. 2 Applied loading

mm strand were selected.

Its taper angle is  $6.47^\circ$ . The wedge taper angle within  $5.7^\circ$  to  $6.33^\circ$  showed adequate performance (Leonhardt 1964). Walsh and Kurama (2010) reported that the optimal angle was  $8.10^\circ$  at the wedge thickness of 13.9 mm for the  $\text{Ø}15.2$  mm strand. The slopes of the existing wedges range between  $7^\circ$  to  $7.5^\circ$  (Cho 2021). Therefore, the taper angle of the wedges can be considered appropriate between  $6^\circ$  and  $8^\circ$ .

Selected wedges are reusable since they were initially developed for the pretensioning method. It is unlikely to reuse the wedges of the PT method as they are buried in the concrete member. Nevertheless, the domestic reusable wedge was chosen because it satisfies both performance and price competitiveness.

## 2.2 Tubular body

The tubular body indicates the central part having a truncated cone-shaped hole where a single strand passes through. The wedges settle on the inclined surface of the hole after biting the strand. The prestressing force is transmitted into compression in concrete at the anchor through wedges.

The initial shape of the tubular body follows the ready-made barrel anchor using the selected wedges (Fig. 1). As the contact area between the wedges and the anchor increases, the surface stress decreases. The width and slope of the hole have a significant effect on the wedge settlement and the hole's geometry remains fixed in the subsequent design process of the current study.

## 2.3 Load

According to ACI 318 (2019), the anchor must not be destroyed or deformed before reaching 95% of the nominal tensile strength of the strand. Considering that an unexpected excessive load may be applied during jacking tendons, the total load is assumed to be 100% of the nominal tensile strength ( $F_p = 258$  kN). Therefore, the average stress is 89.81 MPa, calculated by dividing  $F_p$  by the inclined area of  $2,872.6$  mm<sup>2</sup>. Conservatively, a surface traction of 90 MPa with a direction parallel to the strand is input to the whole inclined surface as shown in Fig. 2.

## 2.4 Materials

GCD 500-7, one of the spheroidal graphite cast iron commonly used for PT anchors along with GCD 400~450, is selected. The material properties of the three specimens are illustrated in Table 1 and they satisfy SPS-KFCA-D4302-5016 (2017).

Table 1 Material properties of casting materials

	Tensile Strength (MPa)	Elongation (%)	Brinell Hardness
GCD 400-18*	≥ 400	≥ 18.0	130~180
GCD 450-10*	≥ 450	≥ 10.0	140~210
GCD 500-7*	≥ 500	≥ 7.0	150~230
Specimen 1	612	9.6	207
GCD 500-7	602	9.8	201
Specimen 2	616	9.6	207
Specimen 3	610	9.7	205
Average	610	9.7	205

\* SPS-KFCA-D4302-5016 (2017)

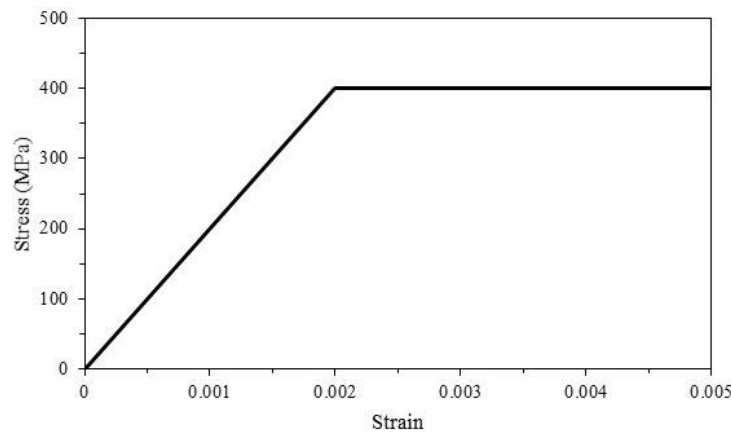


Fig. 3 Applied material property for GCD 500-7 in finite element analysis

The input material properties are also conservatively set as shown in Fig. 3, considering the possible performance degradation during production. The yielding strength is 400 MPa, 80% of the minimum criteria or 66% of the average tensile strength. The elastic modulus is 200,000 MPa, and the Poisson's ratio is 0.3.

### 2.5 Bearing plate

In general, a post-tensioned anchor has a bearing plate while an anchor for pretensioning typically consists of a tubular body itself only. The concrete can be easily damaged by the small bottom area of the tubular body. The bearing plate contributes to enlarging the bearing area so that the bearing stress to the concrete decreases.

For a thin slab of flat plates, the smaller bearing plate size is more advantageous as long as the stress concentration can be avoided.

Cho (2021) investigated the bearing plate sizes of the existing anchors. The length of the anchors for  $\emptyset$  15.2 mm single strands ranges from 105 to 149 mm and the width from 55 to 89 mm. The anchor with the smallest bearing area has the thickest plate. It seems capable of preventing the shear failure of the plate. Although additional steel reinforcement would be located in the anchorage zone, it is recommended to have a sufficient plate area because concrete compressive

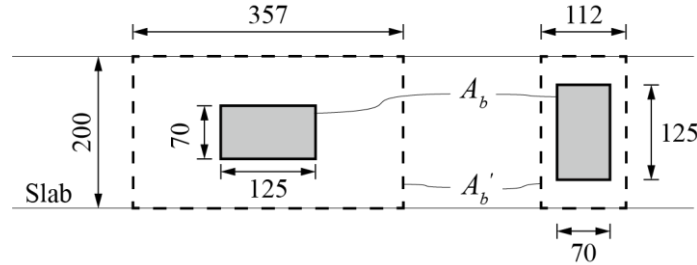


Fig. 4 Bearing area for PT slab (unit: mm)

Table 2 Permissible compressive stress  $f_{cp}$  (unit: MPa)

	At transfer load	At service load
Vertical	30.0	33.6
Horizontal	31.3	35.0

destruction is more vulnerable than the shear of the plate. A double-plate anchor obtains enough bearing area with the two small plates but is too large in overall size.

Given that the typical thickness of the residential PT concrete slab is 200 mm, the anchor design length and width are determined to be 125 mm and 70 mm, respectively, resulting in the anchor plate area of 8,750 mm<sup>2</sup> which is smaller than most of the existing anchors for  $\emptyset 15.2$  mm strands. As the plate dimensions are determined to be reduced, the bearing stress should be examined mathematically as well as experimentally.

The anchorage can be placed vertically or horizontally as shown in Fig. 4. The net bearing area of anchorage  $A_b$  is the total plate area and the maximum bearing area in anchorage zone  $A_b'$  is geometrically proportional to the shape of the anchor plate.

Permissible compressive stresses  $f_{cp}$  calculated by Eqs. (1) and (2) presented in KCI (2010) are illustrated in Table 2. The specified concrete strength  $f_c$  is 35 MPa. The concrete strength at service load  $f_{ci}$  is assumed to be 25 MPa, the minimum value suggested by KCI (2010). In all cases,  $f_{cp}$  exceeds 29.5 MPa, that is  $1.0F_p$  divided by the plate area. Therefore, the length and width of the bearing plate is deemed appropriate.

The initial thickness of the plate is set as 7 mm based on the average of other products. The thickness was optimized during the design process.

$$f_{cp} = 0.75f_{ci}\sqrt{\frac{A_b'}{A_b}} \leq 1.25f_{ci} \quad \text{at transfer load} \quad (1)$$

$$f_{cp} = 0.6f_c\sqrt{\frac{A_b'}{A_b}} \leq f_c \quad \text{at service load} \quad (2)$$

## 2.6 Boundary condition

Theoretically, post-tensioned anchors do not move or rotate until the concrete cracks since they are mostly embedded in concrete. However, the analysis shows minor deformation and stress

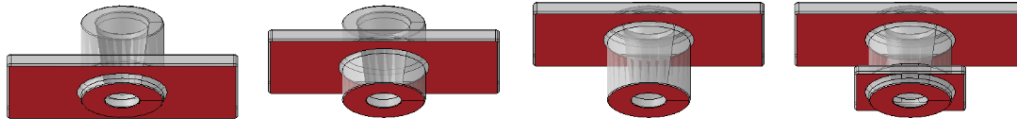


Fig. 5 Fixed boundary condition

Table 3 Location of bearing plate

$h_p$ (mm)	8.5	23.5	40	8.5 & 40
$f_{v,max}$ (MPa)	229.3	223.5	281.1	225.4

S, Mises (Avg: 75%)

223.8E+00

180.0E+00

150.0E+00

140.0E+00

130.0E+00

120.0E+00

110.0E+00

100.0E+00

90.0E+00

80.0E+00

70.0E+00

60.0E+00

50.0E+00

40.0E+00

30.0E+00

20.0E+00

10.0E+00

0.0E+00

when most of the outer surfaces are fixed. It is reasonable that the fixed boundary condition, named ‘Encastre ( $U_1=U_2=U_3=UR_1=UR_2=UR_3=0$ )’ in Abaqus is only applied to the bottom surfaces of the tubular body and the bearing plate (Fig. 5).

### 3. Design optimization through Finite Element Analysis

Design optimization was carried out to have a minimum von Mises stress under the same conditions with only the shape as a variable. The von Mises stress represents the magnitude of the torsional energy of the elements. It is also known as a criterion for accurately predicting severe deformation.

Each model’s maximum von Mises stress ( $f_{v,max}$ ) is measured at each step and the model having the minimum value is selected. Only the results less than 400 MPa are allowed because yielding should not occur during the normal state. Practical reasons are considered simultaneously and a design with minimum stress may not be selected.

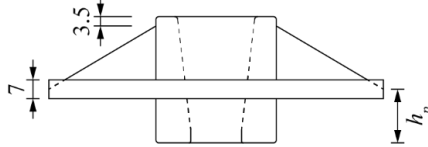
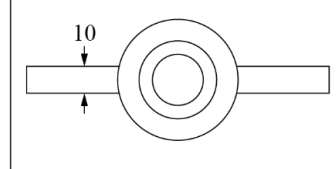
The following design order was conducted according to the importance arbitrarily determined by the authors. Since all design variables are interrelated, some procedures may need to be repeated.

#### 3.1 Location of bearing plate

The location of the bearing plate relative to the wedge-contact surface significantly affects the stress distribution. The wedge-contact surface is inclined, so the pressure from the wedges is transferred diagonally. The bearing plate aids in binding the pressure radiating sideways from the tubular body.

Table 3 shows the analysis results for when the distances from the bottom of the tubular body to the center of the bearing plate,  $h_p$ , are 8.5 mm, 23.5 mm, 40 mm, respectively. It appears to be most effective when the bearing plate is in the middle of the tubular body. The bearing plate at the bottom performs similarly. The bearing plate located at the top does not effectively hold the spreading stress, making it vulnerable to the punching and folding effects and having stress

Table 4 Location of bearing plate with gusset

											
$h_p$ (mm)	16.5	17.0	18.0	19.0	20.0	21.0	22.0	23.0	23.5	27.0	30.5
$f_{v,max}$ (MPa)	224.1	229.7	210.4	208.4	201.6	206.5	232.0	245.6	208.6	225.5	293.0

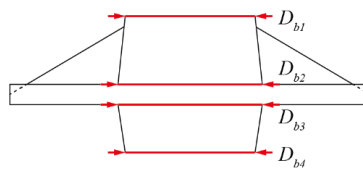


Fig. 6 Variables for the outer diameters of the tubular body

concentrated where the bearing plate and the tubular body meet. However, the stress is significantly reduced when the square plate (60 mm × 60 mm) is added at the bottom.

The bearing plate is relatively thin and sensitive to shear. Gussets located above the plate help restrain the stress that spreads from the tubular body and prevents the shear failure of the plate. So, the bearing plate can be located slightly lower. In order to preferentially reflect the effect of the plate's position rather than the stress dispersion effect by the gusset shape, the initial shape of the two gussets was set as a simple triangle with 10 mm of thickness.

The von Mises stress is first analyzed at 3.5 mm intervals between 16.5 mm to 30.5 mm and then further analyzed at 1 mm intervals in the range of 17 mm to 23 mm. According to Table 4,  $f_{v,max}$  is the smallest when  $h_p$  is 20 mm.

### 3.2 External shape of tubular body

When only the tubular body is considered, the amount of material can be increased by enlarging the diameter over the entire height to raise the resistance. However, since the bearing plate and gussets are attached, stress concentration may occur at the point where each part intersects. As shown in Fig. 6, the tubular body is divided into upper and lower parts based on the bearing plate and each part's top and bottom diameters are used as variables;  $D_{b1}$ ,  $D_{b2}$ ,  $D_{b3}$ , and  $D_{b4}$ . Each diameter ranges from 45 mm to 55 mm and has 5 mm intervals considering the manufacturing.

Rather than each diameter size, the relationships between  $D_{b1}$  and  $D_{b2}$  or  $D_{b3}$  and  $D_{b4}$  show much relevance to the stress distribution (Table 5). When  $D_{b2}$  is larger than  $D_{b1}$ , the truncated cone shaped part above the bearing plate acts similarly as a gusset. If  $D_{b4}$  is smaller than  $D_{b3}$ , the bearing stress increases and the nailing effect may occur. Conversely, if  $D_{b4}$  is greater than  $D_{b3}$ , both the bearing and fixed boundary areas enlarge. As a result, 55-55-45-55 ( $D_{b1}$ - $D_{b2}$ - $D_{b3}$ - $D_{b4}$ ) causes the smallest  $f_{v,max}$  followed by 45-55-45-55. Since it is difficult to manufacture using a mold when  $D_{b3}$  is smaller than  $D_{b4}$ , 45-55-45-45, the one that causes the third smallest stress, was selected in this study.

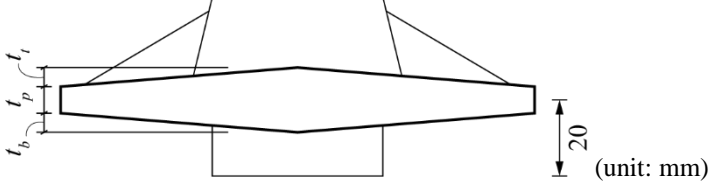
Table 5 Shape of tubular body

$D_{b1}$ (mm)	$D_{b2}$ (mm)	$D_{b3}$ (mm)	$D_{b4}$ (mm)	$f_{v,max}$ (MPa)		
45	45	45	45	207.6		
			50	196.3		
			55	202.3		
		50	45	45	217.8	
				50	197.2	
			55	45	270.7	
				55	205.8	
				45	191.8	
	50	50	45	50	193.7	
			45	45	219.5	
			50	50	195.8	
			45	45	186.6	
		55	45	45	55	184.3
				45	45	252.9
			Continuous linear slope	55	55	193.5
				50	50	196.3
55	45	45	45	203.7		
			50	50	199.7	
			45	45	216.8	
		50	50	50	190.4	
			45	45	201.8	
			50	50	218.7	
	55	50	50	45	203.3	
				50	50	197.5
			Continuous linear slope	45	45	199.7
		45		45	198.5	
		45		55	188.0	
		55	45	55	45	270.6
55	190.2					
55	45			45	188.3	
	55		55	182.2		
Continuous linear slope	45		45	226.4		
Continuous linear slope	45	55	189.6			
Continuous linear slope	45	45	211.1			

### 3.3 Thickness of bearing plate

There are various bearing plate types among existing anchors, such as flat, top convex, and bottom convex. First, a suitable average thickness is verified by an analysis of the flat plates in the

Table 6 Thickness of bearing plate



$t_p$ (mm)	$t_i$ (mm)	$t_b$ (mm)	$f_{v,max}$ (MPa)
3	0	0	215.2
4	0	0	219.1
5	0	0	232.7
		0	186.9
	0	1	400.0
		2	268.3
		3	265.1
6	0.5	0.5	317.0
	1	0	191.9
		1	378.5
	1.5	1.5	296.4
	2	0	186.9
	3	0	191.5
		0	184.2
	0	1	292.9
		2	257.9
7	0.5	0.5	353.4
	1	0	202.0
		1	400.0
	2	0	193.5
	3	0	195.3
8	0	0	188.2
9	0	0	189.8
10	0	0	199.0
11	0	0	199.9
12	0	0	192.5
13	0	0	178.8
14	0	0	181.9

range of 3 to 14 mm. Thin plates with 3 to 5 mm thickness have high stresses while the anchor with 13 mm and 14 mm thickness has a relatively small  $f_{v,max}$ . However, a thick plate over 10 mm makes the anchor bulky and uneconomical. Therefore, it seems suitable at 6 mm or 7 mm where the fourth and third smallest  $f_{v,max}$  is found respectively (Table 6).

Subsequently, the analysis is performed with various forms of bearing plates in the range of 6

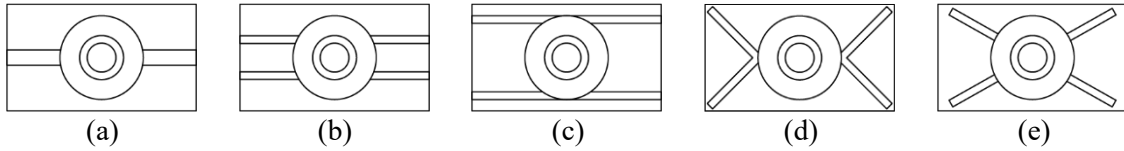


Fig. 7 Examples of gusset arrangement

Table 7 Comparison between curved and triangle gussets

$d_c$ (mm)	Curved	Triangle
0	186.9	193.9
2.5	186.2	190.3
5	185.9	191.0

to 10 mm. The thickness of each end of the plate is 6 or 7 mm. The stress increases significantly in the downward convex form. V-shape of the bottom convex concentrates the stress in the middle of the plate.

Flat plates have lower stress than other convex shapes. Also, the top convex plates are effective in reducing the stress. However, the inclined plate is believed to make it easier to remove the mold during the fabrication process than the flat form. Therefore, the initially selected shape was the top convex with a thickness of 6 mm at both ends and 8 mm at the center.

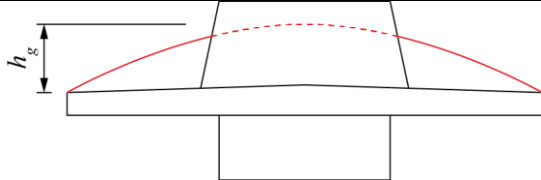
Later, while producing prototypes, it was discovered that the convex shape on both sides is easier for removing the mold than the top convex. Furthermore, the product quality has improved and the defect rate has decreased. Additional analysis with the changed shape was conducted later.

### 3.4 Arrangement of gussets

Stress distribution was examined depending on the gusset shape. There are no restrictions on the gusset shape. It is tough to distinguish the tubular body, the bearing plate, and the gussets in some anchors because they are integrated into a streamlined shape. Since the streamlined anchor requires a large amount of material, plate-type gussets are considered for the optimization.

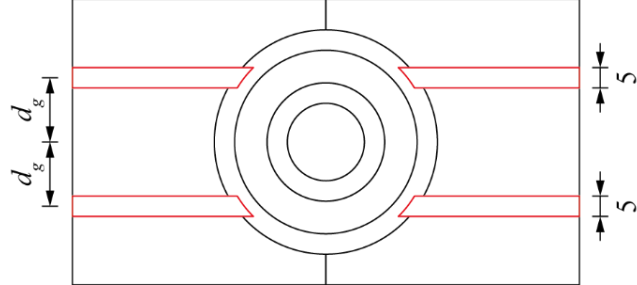
When using plate gussets, the arrangement from the top should be considered. Fig. 7 illustrates examples of gusset arrangements. In option (a), it owns one thick straight line used in the previous analysis but it risks shear failure in the corner. Each thick gusset can be divided into two parallel thin gussets like options (b) and (c). There are also shapes with a diagonal arrangement that distributes the load from the tubular body throughout the bearing plate. Option (d) has two gussets on either side intersected at the outer center of the tubular body. Option (e) gets all four gussets placed radially from the hole center. Both the producing method and cost should be considered in consultation with the manufacturer. It is not easy to manufacture the diagonal layout. Thus, the

Table 8 Height of gusset



$h_g$ (mm)	12	13	14	15	16	17	18	19	20	20.5	24
$f_{v,max}$ (MPa)	190.4	189.2	196.4	189.5	192.2	191.1	190.5	192.8	192.9	197.7	224.1

Table 9 Half distance between parallel gussets



$d_g$ (mm)	2.5	5	7.5	10	12.5	15	17.5	20	22.5	25
$f_{v,max}$ (MPa)	189.2	196.3	187.8	192.0	185.3	187.9	189.1	186.2	187.9	186.6

(unit: mm)

parallel gusset arrangement was chosen.

### 3.5 Front shape of gussets

First, the front shape of the gusset is considered (Table 7). The 3-point arc connects the bearing plate’s top ends and the tubular body’s top center. The straight lines are drawn based on the curve’s points, meeting the tubular body and the top corner of the bearing plate. Here,  $d_c$  denotes the vertical distance between the level at which the curved line or the straight line meets the tubular body and the level at which gussets are truncated horizontally.

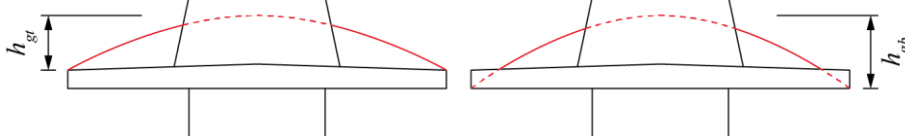
According to the results, curved gussets perform slightly better than straight gussets. Moreover, the truncated gussets show better performance than uncut gussets. However, the truncated gussets have large unnecessary portions of stress not transmitted. Furthermore, the stress concentrates at a junction where the gusset and the tubular body meet.

Since no significant difference is observed in the maximum stress, only the optimum height of the curved gusset is investigated (Table 8). The maximum stress appears to be the smallest when  $h_g$  is 12.5 mm, where  $h_g$  is the height of the gusset from the top edge of the bearing plate.

### 3.6 Distance between parallel gussets

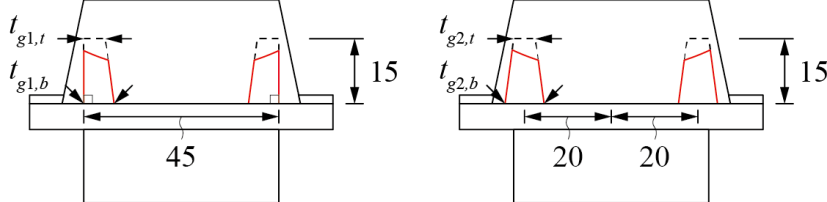
One 10 mm thick straight line can be divided into two 5 mm thick straight lines and the stress change is analyzed according to the distance between the centers of the two lines. The results are shown in Table 9. If the distance between the half of the centers of two gussets ( $d_g$ ) is 2.5 mm, it

Table 10 Curvature of gusset



$h_{gt}$ (mm)	12	13	14	15	16	17	18	19	20	20.5	24
$f_{v,max}$ (MPa)	190.4	189.2	196.4	189.5	192.2	191.1	190.5	192.8	192.9	197.7	224.1
$h_{gb}$ (mm)	18	19	20	21	22	23	24	25	26	26.5	30
$f_{v,max}$ (MPa)	189.1	193.5	191.9	186.6	192.2	189.5	190.3	189.4	191.7	195.2	191.7

Table 11 Thickness of gusset



$t_{g1,t}$ (mm)	$t_{g1,b}$ (mm)	$f_{v,max}$ (MPa)	$t_{g2,t}$ (mm)	$t_{g2,b}$ (mm)	$f_{v,max}$ (MPa)
4	4	197.3	4	4	189.0
	6	190.4		6	188.7
	5	186.6		5	186.6
5	6	187.8	5	6	194.8
	7	190.2		7	189.4
	4	190.9		4	185.2
6	5	194.4	6	5	184.9
	6	187.0		6	199.3
	5	191.4		5	194.8
7	7	197.7	7	7	191.0
	8	188.2		8	189.9
9	9	187.0	9	9	189.5

(unit: mm)

means the two gussets are literally attached, forming a gusset with a thickness of 10 mm. Compared with this, separated gussets are more efficient and distribute the stress more evenly over the bearing plate. The result is most efficient when the distance is 12.5 mm. However, 20 mm, the next best option is selected considering the possible load eccentricity at the edge of the bearing plate.

### 3.7 Front shape of gussets

Since the position of the gussets has been changed, the optimized height of the gusset is found again. On this occasion, all cases where both ends of the 3-point curve meet the upper or lower edges of ends of the bearing plate are taken into consideration. The gusset height,  $h_{gt}$  or  $h_{gb}$ , is

Table 12 Rounding radius between upper tubular body and bearing plate

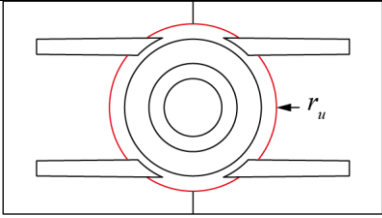
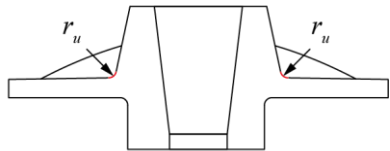
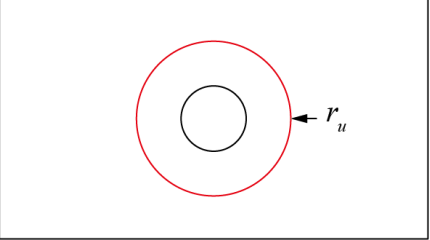
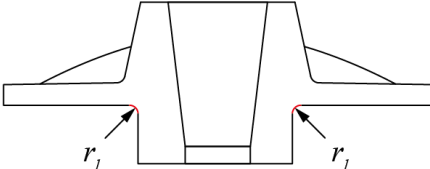
									
$r_u$ (mm)	0.5	1.0	1.5	2.0	2.5	3.0	3.5	4.0	
$f_{v,max}$ (MPa)	186.8	192.1	189.6	194.4	186.6	191.7	189.9	183.8	
$r_u$ (mm)	4.5	5.0	5.5	6.0	6.5	7.0	7.5	8.0	
$f_{v,max}$ (MPa)	185.9	189.6	193.0	186.5	186.8	189.4	191.0	192.2	

Table 13 Rounding radius between lower tubular body and bearing plate

									
$r_l$ (mm)	0.5	1.0	1.5	2.0	2.5	3.0	3.5	4.0	
$f_{v,max}$ (MPa)	340.0	291.0	186.2	183.8	192.7	198.1	193.4	195.9	
$r_l$ (mm)	4.5	5.0	5.5	6.0	6.5	7.0	7.5	8.0	
$f_{v,max}$ (MPa)	196.6	200.3	196.0	204.5	203.0	209.9	243.1	239.4	

defined as the vertical distance between the endpoint and the midpoint of the 3-point curve. The  $h_{gb}$  is 6 mm (the end thickness of the bearing plate) higher than  $h_{gt}$ . According to the results in Table 10, the curve from the bottom edge of the bearing plate is more efficient than that from the top edge. Since the bottom surface of the bearing plate contacts with the concrete, it is found to be more efficient than the force transferred from the tubular body which is then directed to the lower edges of the bearing plate. The shape where  $h_{gb}$  is 21 mm is selected due to the smallest maximum stress.

### 3.8 Thickness of gussets

In this section, the thickness of the gusset is determined (Table 11). As evidenced in the previous analysis, the distance between the centers of the gussets was chosen to be 40 mm and the outer distance to be 45 mm when the gusset thickness was 5 mm. It is similar to the outer diameter at the top of the tubular body. Accordingly, the thickness of the flat gusset  $t_{g1}$  is changed inward. Meanwhile, as shown in the previous analysis, the half distance between the gussets was fixed at 20 mm whereas the thickness of the gusset for that case ( $t_{g2}$ ) was changed. The optimum results were obtained when the gusset thicknesses  $t_{g1}$  and  $t_{g2}$  for both cases were 5 mm (same state).

To elaborate further, the upper and lower thicknesses of the gusset are determined. Both cases

Table 14 Rounding radii for gusset edges

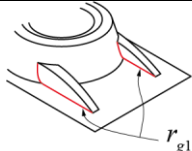
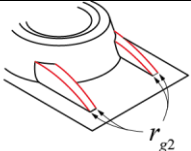
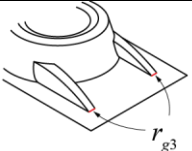
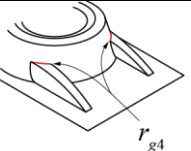
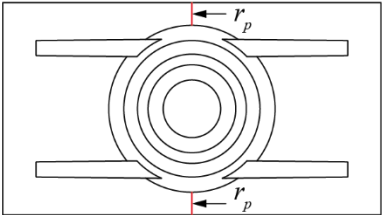
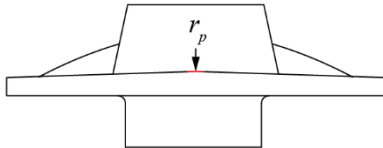
										
$r_{g1}$ (mm)	1	2	3	4	5	6	7	8	9	10
$f_{v,max}$ (MPa)	280.5	212.4	208.8	191.5	181.1	186.8	185.1	191.7	191.3	186.9
$r_{g2}$ (mm)	1	2	3	4	5	6	7	8	9	10
$f_{v,max}$ (MPa)	183.1	186.91	188.4	196.0	191.4	192.4	190.7	181.3	190.8	194.0
$r_{g1}$ (mm)	1	2	3	4	5	6	7	8	9	10
$f_{v,max}$ (MPa)	188.6	185.1	216.1	194.3	189.2	191.8	184.9	198.5	185.6	189.7
$r_{g2}$ (mm)	1	2	3	4	5	6	7	8	9	10
$f_{v,max}$ (MPa)	188.6	188.2	192.4	212.3	201.2	200.5	194.6	278.9	224.9	187.3

Table 15 Rounding radii for bearing plate

									
$r_p$ (mm)	1	2	3	4	5	10	15	20	25
$f_{v,max}$ (MPa)	208.4	187.5	209.0	189.8	189.7	197.8	205.7	190.2	192.6

of the gussets' outer distances of 45 mm and 40 mm are taken into consideration. Since the optimized thickness of the flat gusset is 5 mm, it is analyzed in the range of 4 to 7 mm (Table 11). Notably, the lowest peak stress in the results is with a distance of 40 mm, a thickness of 6 mm on the top, and 5 mm on the bottom.

### 3.9 Radii

A fillet radius redirect stresses from being concentrated at the sharp corner. It also minimizes turbulence in the metal to inhibit formation defects from oxides and trapped gas. Furthermore, radii dissipate heat which improves solidification. For the reasons mentioned above, the corners or edges should be smoothed. The radii are also optimized with a finite element analysis.

First, the boundary between the body and the anchor plate is judged (Tables 12 and 13). This pertains to the efficacy with which the body's power can be distributed to the anchor plate. It is the most efficient when  $r_u$  is 2.5 mm while  $r_l$  is 2 mm where  $r_u$  is the boundary radius between the bearing plate and the upper body and  $r_l$  is the boundary radius between the bearing plate and the lower body.

Next, the edges of the gussets are taken into consideration (Table 14). The part that crosses the gusset, the body, and the bearing plate is optimized at 5 mm ( $r_{g1}$ ). The upper edge of the gusset

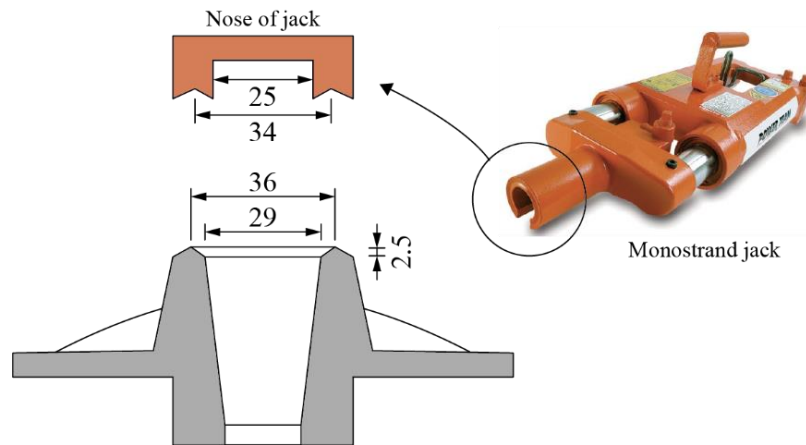


Fig. 8 Nose of the jack and mountain-shaped anchor head (unit: mm)

( $r_{g2}$ ) was found to be most effective at 8 mm but the thickness of the gusset was between 5 mm and 6 mm which is why 2 mm was picked. The optimum radius between the gusset and the bearing plate ( $r_{g3}$ ) was 2 mm. The stress was also the smallest at  $r_{g4}$  of 2 mm where  $r_{g4}$  is the radius between the gusset and the upper body.

Finally, the curvature of the bent portion of the upper convex bearing plate  $r_p$  is analyzed (Table 15). No significant differences are found in the curvature of the naked eye. It was found that 2 mm of them appeared most effectively.

In most cases, the corner curvature of 2 mm was found to be the most helpful. Accordingly, the edges or boundaries not previously determined by the analysis were applied on a 2 mm radius.

#### 4. Consideration for practical construction

The anchor has been designed by conducting a finite element analysis. However, it still needs to be determined whether or not the designed anchor can be used in actual construction. In this section, anchor design is changed to consider the following points.

##### 4.1 Jacking device

When jacking the strand, the nose of the jacking device lends support to the anchor. Therefore, a mountain shape may be required on top of the tubular body. A mountain shape similar to the existing anchors is utilized to ensure versatility with the existing jacks. An existing anchor using an  $\varnothing 12.7$  mm strand (not  $\varnothing 15.2$  mm) is taken into consideration to avoid increasing the size of the anchor. Its mount diameter is 34 mm. However, since the wedge hole diameter of the developing anchor is 29 mm, the mount diameter is determined as 36 mm (Fig. 8). The height of the mountain is 2.5 mm which is the same as that of the existing anchor.

##### 4.2 Endcap

There are several ways of fitting the endcap to safeguard the tendon tail and wedge hole from

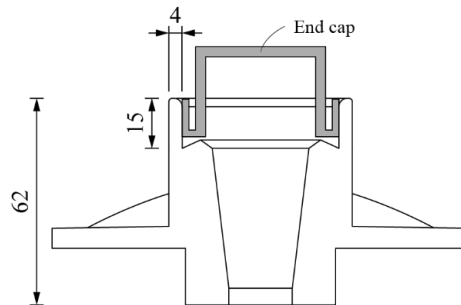


Fig. 9 Anchor head design for endcap (unit: mm)

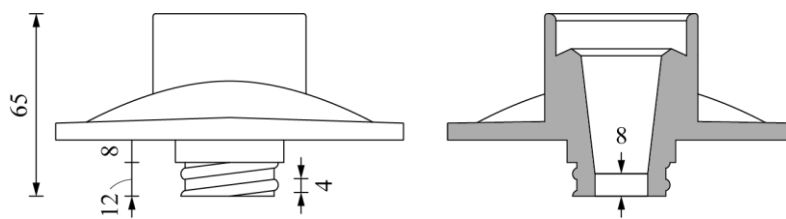


Fig. 10 Redesign of lower body for sleeve (unit: mm)

corrosion. Many anchors use the screw method which is time and energy-intensive depending on the number of threads. By using the push-in method, the worker can easily insert it and drastically shorten the construction time (Fig. 9). Based on the existing 12.7 mm diameter cap, the inner diameter required for capping is 47 mm whereas the minimum required thickness is 4 mm to clean the casting surface. The upper body is a cylinder with a diameter of 55 mm which is already analyzed in Table 5. The end edges of the casting are rounded, implying that the endcap can be easily inserted.

The wall thickness is set as 4 mm. The molten metal requires enough size of gap to traverse, so the mold filling is virtually impossible below 3.2 mm.

#### 4.3 Sleeve

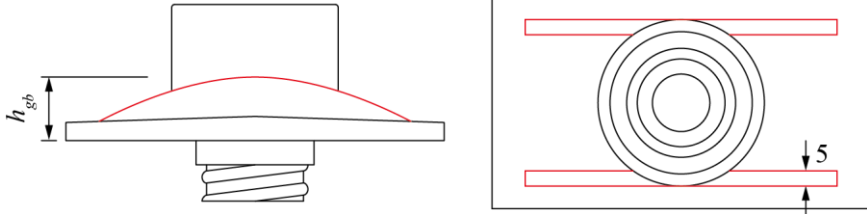
The screw-in type can securely fix the sleeve to prevent it from falling out. In addition, it is excellent when it comes to waterproofing since it is formed to cover the inside of the anchor.

Water-tightness improves when there are many threads with small gaps but the workability is significantly reduced. The round thread is applied so that the sleeve can be easily inserted even when the casting finishing may not be clean. As shown in Fig. 10, the screw length is 12 mm and the distance between the thread pitches is 8 mm. The sleeve can be fitted with only 1.5 rotations, thus, reducing the work time.

Applying threads for the sleeve, the vertical section of the wedge cavity increased from 5 mm to 8 mm. Increasing this interval is simply an increase in the free length of the strand. In this regard, Walsh and Kurama (2010) found that the change in free length does not affect anchorage settlement.

On the other hand, the lower body's outer part is changed into a screw shape. There is a possibility of a stress concentration occurring here which was verified through analysis in Section 4.4.

Table 16 Height of gusset with design changes

	(unit: mm)										
$h_{gb}$ (mm)	18	19	20	21	22	23	24	25	26	26.5	30
$f_{v,max}$ (MPa)	258.7	276.9	264.8	257.6	259.9	281.9	275.0	261.1	278.9	266.0	291.6

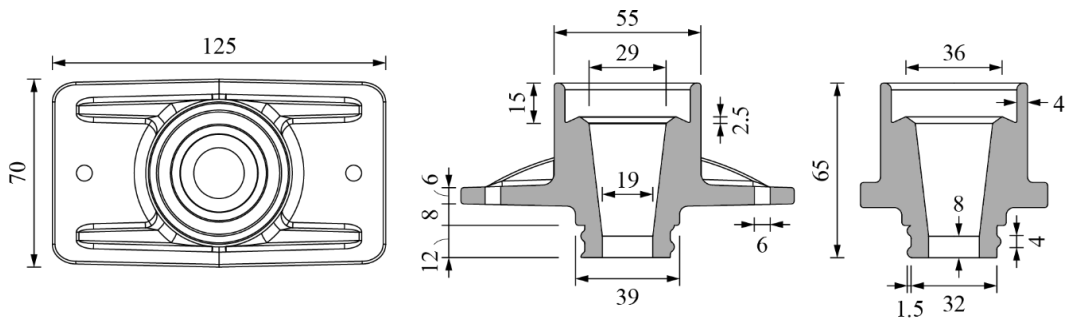


Fig. 11 Drawings of designed bare anchor (unit: mm)



(a) bare anchor



(b) accessories

Fig. 12 Developed bare PT anchorage

#### 4.4 Casting fabrication

The mold must be able to fall out of the casting easily. Therefore, the middle part of the anchor is thick and becomes thinner toward the end in removing the mold frame. Since the anchor has a screw part where the sleeve is fitted, a total of three parts of the mold are used. Especially, the bearing plate and the gussets should be inclined smoothly.

The shape of the anchor plate selected through the finite element analysis is thin at both ends and thick in the middle, flat at the bottom, and convex at the top. However, it is changed to convex at the top and bottom to form the slope. Given that there is no significant difference in the efficiency of the anchor depending on the type, the thickness of both ends and the middle part remain the same as that of the finite element analysis which implies that the amount of casting

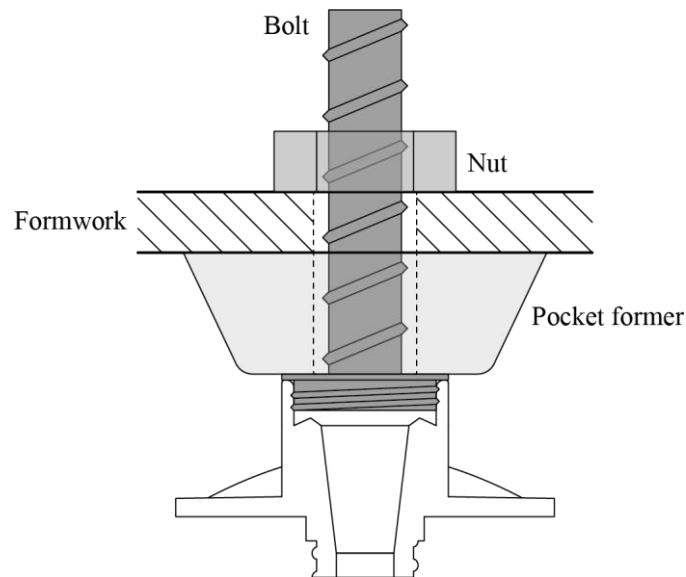


Fig. 13 Bolt-nut type of pocket former

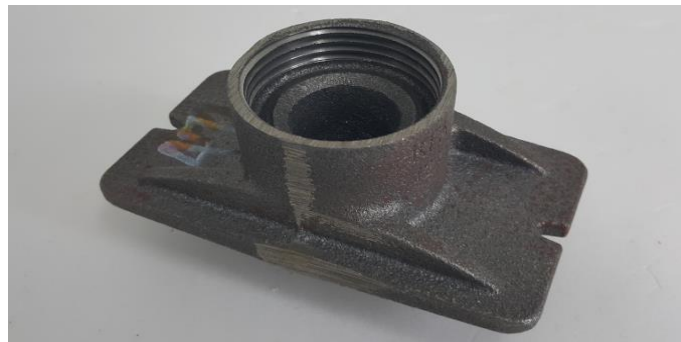


Fig. 14 Modified bare PT anchor

hardly changes.

Fig. 11 illustrates a drawing of a bare anchor developed by considering the finite element analysis results and constructability. The overall shape, except for screw threads, is symmetrical and is slightly tapered outwards for fabrication.

The prototype is as shown in Fig. 12(a). The material of the casting is GCD 500-7. Fig. 12(b) depicts the accessories used as a set and their fittings in the anchorage. The sleeve is threaded as previously designed. The pocket former is inserted into the anchor head and fixed by nails through the holes. The endcap can be fitted to the anchor head and remains tight without any additional fixing.

#### 4.5 Pocket former

The conventional method for fixing a pocket former is inefficient, thus, underpinning the need for using the bolt nut method (Fig. 13) for the gang-form system. The bolt-nut method refers to a

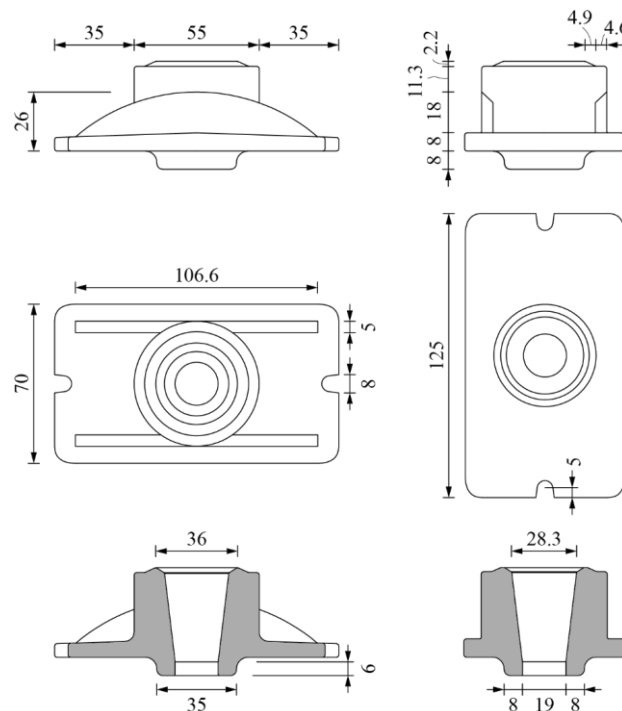


Fig. 15 Drawings of bare casting for the encapsulated system (unit: mm)

method of inserting a plastic bolt in the anchor head, inserting a pocket former, and then tightening a plastic nut from the outside of the formwork. The anchor can always be positioned perpendicular to the formwork because the bolt passes the hole drilled in the formwork. Additionally, the anchorage can be fixed to the formwork only using bolts and nuts without nails. The same formwork or gang-form can be reused to improve the workability if the tendon profile remains unchanged across several floors. The pocket former, bolt, and nut are reusable unless each one is deformed or broken.

Accordingly, the pocket former is modified to consist of bolts, nuts, and pockets. Then, as shown in Fig. 14, threads are further machined inside the anchor head to secure the bolts to the anchor. A groove was formed in the center of both ends of the bearing plate to fix with nails or screws. Such classical methods can be applied when deemed necessary.

## 5. Design for encapsulated anchor

### 5.1 Need for encapsulated system

ACI 423.7 (2014) mandates the encapsulation system for all PT anchors governed by either ACI 318 (2019) or ACI 350 (2006). The plastic coating minimizes the corrosion of the casting from direct contact with concrete and water. Therefore, encapsulation anchorages are strongly recommended not only in harsh environments and may also be in general circumstances.

Encapsulation is not yet mandatory in Korea. However, the corrosion issues of prestressing



Fig. 15 Drawings of bare casting for the encapsulated system (unit: mm)

tendons have been raised steadily in Korea. So, the encapsulated system is applied to the developed PT anchor to improve the long-term behavior of buildings.

### 5.2 Encapsulated anchor and accessories

In addition to structural parts, a bare anchor requires additional castings to apply accessories. However, unnecessary portions of the casting can be minimized by replacing them with plastic.

The drawings of the modified bare anchor are depicted in Fig. 15. The threaded portion for inserting the pocket former or endcap is cut. The screw for the sleeve is removed which reduces the height of the lower body. Therefore, the total height of casting is only 47.5 mm. Unlike the original bare anchor, the modified anchor cannot use accessories by casting itself and must undergo the encapsulation process.

Fig. 16 illustrates the encapsulated anchor. The plastic material is linear low-density polyethylene (LLDPE) and the thickness of the plastic cover is 2 mm. When the cover is hard, it is durable in scratching but the cracks may occur even in the case of a small deformation. Otherwise, it is not broken by impact or deformation with soft plastic. However, workability may deteriorate because the parts for the pocket former, sleeve, or endcap are bent under weak force. Therefore, a proper compounding of the plastic material is found and verified through a mock-up test. In addition to encapsulation, this can also be applied on the plastic-formed pocket formers and endcaps, thereby increasing the applicability of accessories.

The sleeve is plastic-molded along with the plastic cover of an anchor as an integrated encapsulation system. The sleeve length is 145 mm which is longer than the minimum length of 100 mm in ACI 423.7 (2010). The diameter decreases towards the end along with a reduction in thickness. The thickness at the sleeve tip is 1.5 mm, thus, exceeding the minimum thickness of 1.27 mm specified in ACI 423.7 (2010).

The cylindrical cover extends about 12 mm from the anchor head to fit the pocket former and endcap. The protruding portion has a thickness of up to 6 mm. The inside has a thread about 2 mm thick to screw the pocket former bolt along with the endcap.

## 6. Conclusions

For designing the anchor, a finite element analysis is performed to investigate the maximum von Mises stress by varying the shape of the tubular body, the bearing plate, and gussets. The shape is optimized to minimize this stress in consideration of a jacking device, accessories, and

workability. ACI 423.7-14, alternatively, requires the use of an encapsulation system that is highly resistant to corrosion. Despite not being mandatory in Korea, the encapsulated anchor was developed to enhance the durability of PT tendons and buildings.

The design results of the bare and encapsulated anchors are summarized as follows.

- Developed bare anchor for Ø15.2 mm stands has a bearing plate of 125 mm × 70 mm with its height being 65 mm.
- The casting material is GCD500-7 and the sleeve can be fixed with threads.
- For the encapsulated anchor, unnecessary casting parts were eliminated because the plastic cover can either substitute or fix the accessory. The height of encapsulated anchor was reduced to 47.5 mm by removing the threaded portion for the sleeve and the cylindrical part for the pocket former/end cap.
- The plastic cover had a thickness of about 2 mm and was made in a single piece including a 145 mm long sleeve. The pocket former and the end cap can be screwed on the anchor head.

## Acknowledgments

This work was supported by the Samsung C&T, National Research Foundation of Korea (grant number NRF- 2018R1D1A1B06044752), and Institute of Construction and Environmental Engineering at Seoul National University, as well as Dongyang Mirae University.

## References

- ACI 318 (2019), *Building Code Requirements for Structural Concrete and Commentary*, American Concrete Institute, Farmington Hills, MI, U.S.A.
- ACI 350 (2006), *Code Requirements for Environmental Engineering Concrete Structures and Commentary*, American Concrete Institute, Farmington Hills, MI, U.S.A.
- ACI 423.7 (2014), *Specification for Unbonded Single-Strand Tendon Materials*, American Concrete Institute, Farmington Hills, MI, U.S.A.
- Cho, A.S. (2021), *Development and Performance Verification of Post-Tensioned Anchor for Unbonded Single-Strand Tendon*, Ph.D. Dissertation, Seoul National University, Seoul, Republic of Korea.
- Cho, A.S., Jo, Y.W., Jeon, B.K. and Kang, T.H.-K. (2015), “Development and performance test for unbonded post-tensioned anchor”, *J. Korea Concrete Institute*, **27**(1), 11-20. <https://doi.org/10.4334/JKCI.2015.27.1.011>.
- Cho, A.S. and Kang, T.H.-K. (2018), “Load-carrying performance and hydrostatic tests of encapsulated anchor systems for unbonded post-tensioning single-strands”, *Int. J. Concrete Struct. Mater.*, **12**. <https://doi.org/10.1186/s40069-018-0233-z>.
- Choi, S.-H., Hwang, J.-H., Han, S.-J., Joo, H.-E. and Kim, K.S. (2021), “Experimental study of punching shear in post-tensioned slabs with unbonded tendons”, *Struct. Eng. Mech.*, **79**(4), 507-516. <https://doi.org/10.12989/sem.2021.79.4.507>.
- Han, S.W., Kee, S.-H., Park, Y.-M., Lee, L.-H. and Kang, T.H.-K. (2006), “Hysteretic behavior of exterior post-tensioned flat plate connections”, *Eng. Struct.*, **28**(14), 1983-1996. <https://doi.org/10.1016/j.engstruct.2006.03.029>.
- Ibrahim Ary, M. and Kang, T.H.-K. (2012), “Shear-strengthening of reinforced & prestressed concrete beams using FRP: part I – review of previous research”, *Int. J. Concrete Struct. Mater.*, **6**, 41-47. <https://doi.org/10.1007/s40069-012-0004-1>.
- Leonhardt, F. (1964), *Prestressed Concrete; Design and Construction*, (2nd Edition), W. Ernst.

- Kang, T.H.-K. and Ibrahim Ary, M. (2012), "Shear-strengthening of reinforced & prestressed concrete beams using FRP: part II – experimental investigation", *Int. J. Concrete Struct. Mater.*, **6**, 49-57. <https://doi.org/10.1007/s40069-012-0005-0>.
- Kang, T.H.-K. and Wallace, J.W. (2008), "Seismic performance of reinforced concrete slab-column connections with thin plate stirrups", *ACI Struct. J.*, **105**(5), 617-625.
- KCI (2010), *Standard Concrete Specification and Commentary*, Korea Concrete Institute, Korea.
- Kim, J.-M., Lee, J. and Sohn, H. (2018), "Detection of tension force reduction in a post-tensioning tendon using pulsed-eddy-current measurement", *Struct. Eng. Mech.*, **65**(2), 129-139. <http://dx.doi.org/10.12989/sem.2018.65.2.129>.
- SPS-KFCA-D4302-5016 (2017), *Spheroidal Graphite Iron Castings*, Korea Foundry Cooperative Association. Korea.
- Twigden, K.M. and Henry, R.S. (2019), "Snap back testing of unbonded post-tensioned concrete wall systems", *Earthq. Struct.*, **16**(2), 209-219. <https://doi.org/10.12989/eas.2019.16.2.209>.
- Walsh, K.Q. and Kurama, Y.C. (2010), "Behavior of unbonded posttensioning monostrand anchorage systems under monotonic tensile loading", *PCI J.*, **55**(1), 97-117. <https://doi.org/10.15554/pcij.01012010.97.117>.
- Yim, H.J., Yang, J.M. and Kim, J.K. (2018), "Improved prestressed concrete girder with hybrid segments system", *Struct. Eng. Mech.*, **65**(2), 183-190. <https://doi.org/10.12989/sem.2018.65.2.183>.
- Zhang, Y., Xu, D. and Liu, C. (2018), "Behavior and stress check of concrete box girders strengthened by external prestressing", *Comput. Concrete*, **22**(2), 133-142. <https://doi.org/10.12989/cac.2018.22.2.133>.